Construction and Building Materials 220 (2019) 206–213

Contents lists available at ScienceDirect

Construction and Building Materials

journal homepage: www.elsevier.com/locate/conbuildmat

Self-cleaning coatings based on fly ash and bismuth-photocatalysts: Bi_2O_3, $Bi_2O_2CO_3$, BiOI, $BiVO_4$, $BiPO_4$

E. Luévano-Hipólito [a], L.M. Torres-Martínez [b,*], L.V.F. Cantú-Castro [b]

[a] CONACYT – Facultad de Ingeniería Civil-Departamento de Ecomateriales y Energía, Cd. Universitaria Universidad Autónoma de Nuevo León, C.P. 66455 San Nicolás de los Garza, NL, Mexico
[b] Facultad de Ingeniería Civil-Departamento de Ecomateriales y Energía, Cd. Universitaria Universidad Autónoma de Nuevo León, C.P. 66455 San Nicolás de los Garza, NL, Mexico

HIGHLIGHTS

- Self-cleaning coatings were fabricated with Bi-photocatalysts and fly ashes.
- $Bi_2O_2CO_3$-coating exhibited the best performance (49%) for self-cleaning on concrete.
- Low crystallite size and high surface area promoted higher efficiencies.
- Self-cleaning activity of coating was restored with water after 28 days of curing.

GRAPHICAL ABSTRACT

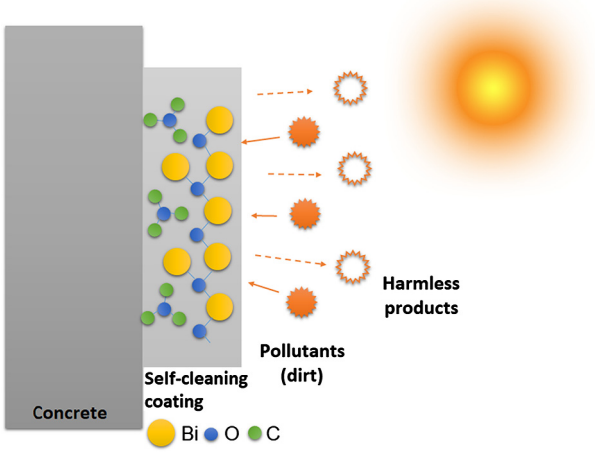

ARTICLE INFO

Article history:
Received 21 March 2019
Received in revised form 13 May 2019
Accepted 3 June 2019
Available online 10 June 2019

Keywords:
Fly ash
Self-cleaning
Photocatalysis
Visible-light photocatalysts
Photocatalytic coating

ABSTRACT

Recently, the design of photocatalytic building materials for self-cleaning, self-disinfecting, and environmental pollution remediation has resulted in increasing interest. The advantage of using solar energy and rainwater as driving force has opened a new domain for environmentally friendly building materials. This work reports the fabrication of photocatalytic self-cleaning coatings with alternative building materials such as fly ash, sodium carbonate as an alkaline activator, and bismuth-based photocatalysts deposited on concrete. The photocatalytic materials were powders of Bi_2O_3, $Bi_2O_2CO_3$, BiOI, $BiVO_4$, $BiPO_4$, which were synthetized by a precipitation method at room temperature without the use of surfactants or additives. The photocatalytic self-cleaning efficiency of the coatings was evaluated according to the ISO 10678:2010 norm by using aqueous methylene blue (MB) as a model pollutant in order to measure the photoactive surface's ability to degrade dissolved organic molecules under light irradiation. The tendency of the photocatalytic self-cleaning coating activities was: $Bi_2O_2CO_3$ (49%) > BiOI (30%) > $BiVO_4$ (15%) > $BiPO_4$ (14%) > Bi_2O_3 (5%) after 3 h of reaction. The best result was obtained when $Bi_2O_2CO_3$ was incorporated into the coatings, and it was associated to its lowest crystallite (27 nm), flake-like morphology, and to its negatively charged surface (pH_{PZC} = 11.5) at the pH of the experiments, that favored the adsorption of the cationic dye (MB) on its surface. The self-cleaning efficiency of the $Bi_2O_2CO_3$ coating was investigated at different curing ages: 7, 14, and 28 days. It was observed a decrement in the

* Corresponding author.
E-mail address: lettorresg@yahoo.com (L.M. Torres-Martínez).

https://doi.org/10.1016/j.conbuildmat.2019.06.030
0950-0618/© 2019 Elsevier Ltd. All rights reserved.

photocatalytic activity with increasing the curing age. However, it was possible to restored the self-cleaning efficiency after washing the surface with water due to the removal of hydration products, which filled up the coating-pores forming diffusion barriers to both reactants and photons.

© 2019 Elsevier Ltd. All rights reserved.

1. Introduction

The incorporation of photocatalysts in building materials to provide a self-cleaning effect offers a wide range of opportunities to ensure proper functionality maintenance over time [1–3]. Furthermore, the self-cleaning effect on building materials provides the possibility of improving the air quality by removing air pollutants such as NO_x, VOCs, and C_7H_8 [4–6]. In this context, TiO_2 is the most used photocatalyst material for self-cleaning applications. The fabrication of photocatalytic self-cleaning coatings with TiO_2 has been demonstrated on different surfaces such as stucco [4], mortars [6], paints [6], and tiles [7]. However, since TiO_2 only absorbs a small part of the light of the solar spectrum (<4%) its activation in outdoor conditions is limited. As an alternative, several efforts have been carried out in order to utilize the visible light from the solar spectrum, such as the modification of TiO_2 with transition metals or non-metallic anionic species [5–10]. In this context, Mosquera et al. synthesized composites based on SiO_2-TiO_2 with small amounts of precious metals (Ag and Au), which were added on stones [8,9]. They found a good synergy and a high self-cleaning efficiency between the semiconductor and the precious metals under visible light irradiation. Also, Cohen et al fabricated a Portland cement blended with Titanium Oxynitride ($TiO_2 - xN_y$) nanoparticles with self-cleaning ability (40%) under visible light activation [10]. Alternatively, $LiNbO_3$ and WO_3/TiO_2 have been coated on concrete for self-depolluting surface [11,12].

Recently, bismuth-based materials have been proposed as alternative visible-light active photocatalysts to the traditional TiO_2, which activity has been probed in the removal of several pollutants of water (rhodamine B, methyl orange, methylene blue) and air (NO_x, VOCs) [13–20,21–23]. In particular, Bi_2WO_6, and Bi_4MoO_9, $BiPO_4$ integrated in core–shell structure with Bismuth metal have resulted in excellent results for NO_x removal from diluted streams [24–26]. There are many advantages of the use of bismuth-based materials in photocatalytic reactions, i.e., these compounds can be activated with the visible light of the solar spectrum since their electronic structure consist in a valence band of hybrid orbitals O *2p* and Bi *6s* [20]. This phenomenon results in an increase in the mobility of photogenerated charge carriers and a decrement of the band gap energy, which increase the photocatalytic activity. In addition, these compounds are related to cost-effectiveness due to their abundance, low toxicity and high stability [27]. However, in spite of the good properties of bismuth-based photocatalysts, their incorporation in building materials has not been reported, so far.

On the other hand, in recent years, the use of alternative cementitious materials has represented a good alternative to replace the Portland cement in coatings that do not need high mechanical resistances, i.e. in facades [28–30]. This alternative represents several advantages such as, reducing the CO_2 emissions involved during the cement fabrication, lowering costs, and in some cases, improving one or more technical properties of concrete. These alternative materials include fly ash, ground granulated blast furnace slag, silica fume, limestone dust, rice husk ash, palm oil fuel ash, cement kiln dust, and metakaolin [31,32]. Among them, fly ash is a combustion by-product generated in coal-burning power plants, which is removed by a dust collection system. Eventually, the disposal of these ashes in landfills can have a negative impact on the environment. Thus, several efforts have been carried out in order to take advantage of these residues. One alternative is the incorporation of fly ash in building materials that can improve some properties such as workability, compressive strength, reduced heat of hydration, decreased costs, and increased resistance to alkali-silica, and sulfates [33–35]. Therefore, the utilization of fly ash as a binder to fabricate self-cleaning ceramic coatings is a topic of interest. This work proposes the fabrication of a photocatalytic self-cleaning coating in order to be applied on concrete surfaces. The coatings were obtained with low cost materials based on the utilization of fly ashes and bismuth compounds active under visible light (Bi_2O_3, $Bi_2O_2CO_3$, BiOI, $BiVO_4$, and $BiPO_4$).

2. Experimental

2.1. Synthesis of photocatalysts

The synthesis of bismuth-based photocatalysts was performed by a facile precipitation method using inorganic salts and avoiding the use of harmful chemical compounds such as surfactants and solvents. All the materials were obtained at 100 °C.

2.1.1. Synthesis of Bi_2O_3

In a typical procedure, 0.05 mol of bismuth nitrate ($Bi(NO_3)_3 \cdot 5H_2O$, Aldrich, 99%) was dissolved in 50 mL of HNO_3 (1 M) until complete dissolution of the inorganic salt. Then, the pH was adjusted to 7 by using NaOH, and the resulting yellow suspension was maintained under vigorous stirring for 1 h. Lastly, the mixture was washed with water and methanol to finally being dried at 100 °C.

2.1.2. Synthesis of $Bi_2O_2CO_3$

The synthesis of $Bi_2O_2CO_3$ involved the preparation of two solutions: 1) 0.05 mol of $Bi(NO_3)_3 \cdot 5H_2O$ was dissolved in HNO_3 (1 M), and 2) stoichiometric amounts of Na_2CO_3 (Aldrich, 99%) were dissolved in distilled water. The solution (1) was added into the second solution until the formation of a white suspension, which was maintained under vigorous agitation for 1 h and then it was washed several times with water and methanol. Finally, the powders were dried at 100 °C.

2.1.3. Synthesis of BiOI

Powders of BiOI were prepared by means of two solutions: 1) 0.05 mol of $Bi(NO_3)_3 \cdot 5H_2O$ was dissolved in 50 mL of ethanol (DEQ, 99%), and 2) stoichiometric amounts of potassium iodide (KI, DEQ, 99%) in 50 mL of deionized water. The solution (1) was poured into the second solution until the formation of a reddish suspension, which was maintained under vigorous agitation for 1 h. Then, the powders were washed several times with water and methanol in order to remove the by-products generated, which were dried at 100 °C.

2.1.4. Synthesis of $BiVO_4$

For this purpose, in a first step 0.05 mol of $Bi(NO_3)_3 \cdot 5H_2O$ was dissolved in 50 mL of HNO_3 (1 M), and stoichiometric amounts of ammonium vanadate (NH_4VO_3, Aldrich, 99%) were added into the solution until the formation of a yellow-orange suspension. The pH was adjusted to 7 by using NaOH, and the resulting suspension

was maintained under vigorous agitation for 1 h. Later, the suspension was washed several times with water and methanol in order to remove the by-products. The powders were dried at 100 °C.

2.1.5. Synthesis of $BiPO_4$

To obtain $BiPO_4$, 0.05 mol of $Bi(NO_3)_3{\cdot}5H_2O$ was dissolved in 50 mL of HNO_3 (1 M) and after complete dissolution of the salt, stoichiometric amounts of ammonium phosphate [$(NH_4)_2HPO_4$, Aldrich, 99%) were added into the solution. Then, the pH was adjusted to 7 by using NaOH, and the resulting powders were washed with water and methanol.

2.2. Preparation of photocatalytic coatings

Fly ash (as a binder), Na_2CO_3, H_2O, and bismuth compounds were used as raw materials to prepare the photocatalytic coating. Fly ashes were provided by a local steel company; whose composition was reported in a previous work [36]. Beforehand, the iron from the fly ashes was removed by magnetic separation, and the resulting ashes were ground in an agate mortar. The ashes were mixed with Na_2CO_3 and H_2O in order to accomplish their alkaline activation. Then, appropriate amounts of photocatalysts were used in the above mixture in order to provide the self-cleaning effect. The weight ratio of the components was 1:0.03:0.33:0.04 of FA: Na_2CO_3:H_2O:Photocatalyst. The hydraulic mixture was applied with a spatula in a concrete surface (previously moistened) of 5 cm of diameter.

2.3. Characterization of photocatalysts

The structural characterization was carried out by X-ray powder diffraction using a Bruker D8 Advance diffractometer with Cu K_α radiation (40 kV, 30 mA). A typical run was made between the 2Θ angles from 10° to 70° with a step size of 0.05° and a dwell time of 0.5 s. The morphology of the photocatalysts was analyzed by scanning electron microscopy (FEI Nova NanoSEM 200 with an accelerating voltage of 30 kV). The UV–Vis diffuse reflectance absorption spectra of the samples were obtained using an Agilent Technologies UV–Vis–NIR spectrophotometer model Cary 5000 series equipped with an integrating sphere. The energy band gap values (E_g) were calculated by converting the reflectance spectra obtained by means of Kubelka-Munk function. The band energy diagrams were calculated according to a procedure suggested by Butler and Ginley [37], taking into account the electronegativity and the band gap obtained by the diffuse reflectance spectra. The BET surface area measurements were carried out by N_2 adsorption–desorption isotherms by means of a Bel-Japan Minisorp II surface area and pore size analyzer. The isotherms were evaluated at −196 °C after pretreatment of the samples at 150 °C for 24 h. Zeta potential determination was measured using a slurry of 0.4 g of the scheelite Nanotrac Flex model DLS 180, using a solution 0.1 M of both HCl and NaOH.

2.4. Photocatalytic activity

Self-cleaning performance of the photocatalytic coating was evaluated following the ISO 10678:2010. In these experiments, a 50 mL cylinder with a diameter of 3.5 cm was attached on the surface of the samples using silicon glue. Then, samples placed in a dark environment for 24 h with 30 mL of an aqueous methylene blue (MB) solution of 10 μmol L^{-1}. This procedure was necessary because the coatings could adsorb the dye molecules. After conditioning, the samples were irradiated with a halogen lamp of 50 W, which emits between 300 and 900 nm. This lamp was chosen in order to simulate the sunlight spectrum. The degradation of MB solution was measured every 10 min (up to 3 h) using a UV–Vis–NIR spectrophotometer model Cary 5000 by determining the maximum absorption spectrum at 665 nm wavelength. For comparative purposes, the photocatalytic activity of powders was measured in a cylindrical batch reactor of 100 mL with the same MB concentration.

3. Results and discussion

3.1. X-ray diffraction characterization

Fig. 1 shows the X-ray diffraction patterns of the bismuth-based photocatalysts obtained at 100 °C. The reflections of photocatalysts were indexed to the following JCPDS Cards: 41-14991 (α-Bi_2O_3), 41-1488 ($Bi_2O_2CO_3$), 73-2062 (BiOI), 14-0133 ($BiVO_4$), 15-0766 ($BiPO_4$). All the materials were obtained in pure form, without the presence of extra reflections. Most of the material crystallized in the tetragonal system, with the exception of the monoclinic α-Bi_2O_3 and hexagonal $BiPO_4$ (Table 1). In particular, α-Bi_2O_3 and $BiPO_4$ are thermodynamically favored at room temperature. Both presented bigger crystallite sizes (65–68 nm) compared to the tetragonal phases. $BiVO_4$ and BiOI showed similar sizes (~46 nm), while $Bi_2O_2CO_3$ exhibited the lowest crystallite size (27 nm) among the studied compounds.

3.2. Scanning electron microscopy

The morphology of the photocatalysts was analyzed by scanning electron microscopy. As it is shown in Fig. 2, a variety of morphologies was obtained in each photocatalysts with the synthesis method proposed, which avoids the use of surfactants or solvents of high toxicity.

The samples with higher crystallite sizes (α-Bi_2O_3 and $BiPO_4$) exhibited a heterogeneous morphology with a notable degree of agglomeration among its particles (Fig. 2a-b, 2i-j). On the contrary, the rest of the samples developed a more homogeneous morphology, which resulted in flakes ($Bi_2O_2CO_3$, Fig. 2c-d), flowers (BiOI, Fig. 2e-f), and spheres ($BiVO_4$ Fig. 2g-h). Among these samples, $Bi_2O_2CO_3$ resulted in the lowest particle size (<100 nm).

3.3. Diffuse reflectance spectroscopy

Fig. 3 shows diffuse reflectance spectra taken for each photocatalyst. Three materials absorb in the visible range of the solar spectrum (Bi_2O_3, BiOI, and $BiVO_4$), while the samples: $Bi_2O_2CO_3$ and $BiPO_4$ absorb in the UV part. Based on extrapolations of the straight portions of the absorption edge, the band gap of the photocatalysts can be estimated, which tendency was: $BiPO_4$ (4.1 eV) > $Bi_2O_2CO_3$ (3.3 eV) > Bi_2O_3 (2.8 eV) > $BiVO_4$ (2.7 eV) > BiOI (2.0 eV) (Table 1). From these data, it was obtained the theoretical band edge energy positions, which are shown in Fig. 4. As can be seen, all the materials have the required thermodynamic potential to generate hydroxyl radicals (·OH) that can oxidize a wide number of organic and inorganic tropospheric pollutants [38,39]. Especially, $Bi_2O_2CO_3$ and $BiPO_4$ had a more positive potential to produce the hydroxyl radicals. However, the activation of $BiPO_4$ could be difficult due to its wide band gap energy (>4 eV), considering the lamp used. All these photocatalysts are classified as bismuth (III) semiconductors, which contribution of Bi 6 s and O 2p levels forms a preferable hybridized valence band while the conduction band is composed of Bi 6p orbitals [40].

3.4. Nitrogen physisorption

N_2 isotherms of the bismuth-photocatalysts are shown in Fig. 5. The profile of the isotherms of Bi_2O_3, BiOI, $BiVO_4$, and $BiPO_4$

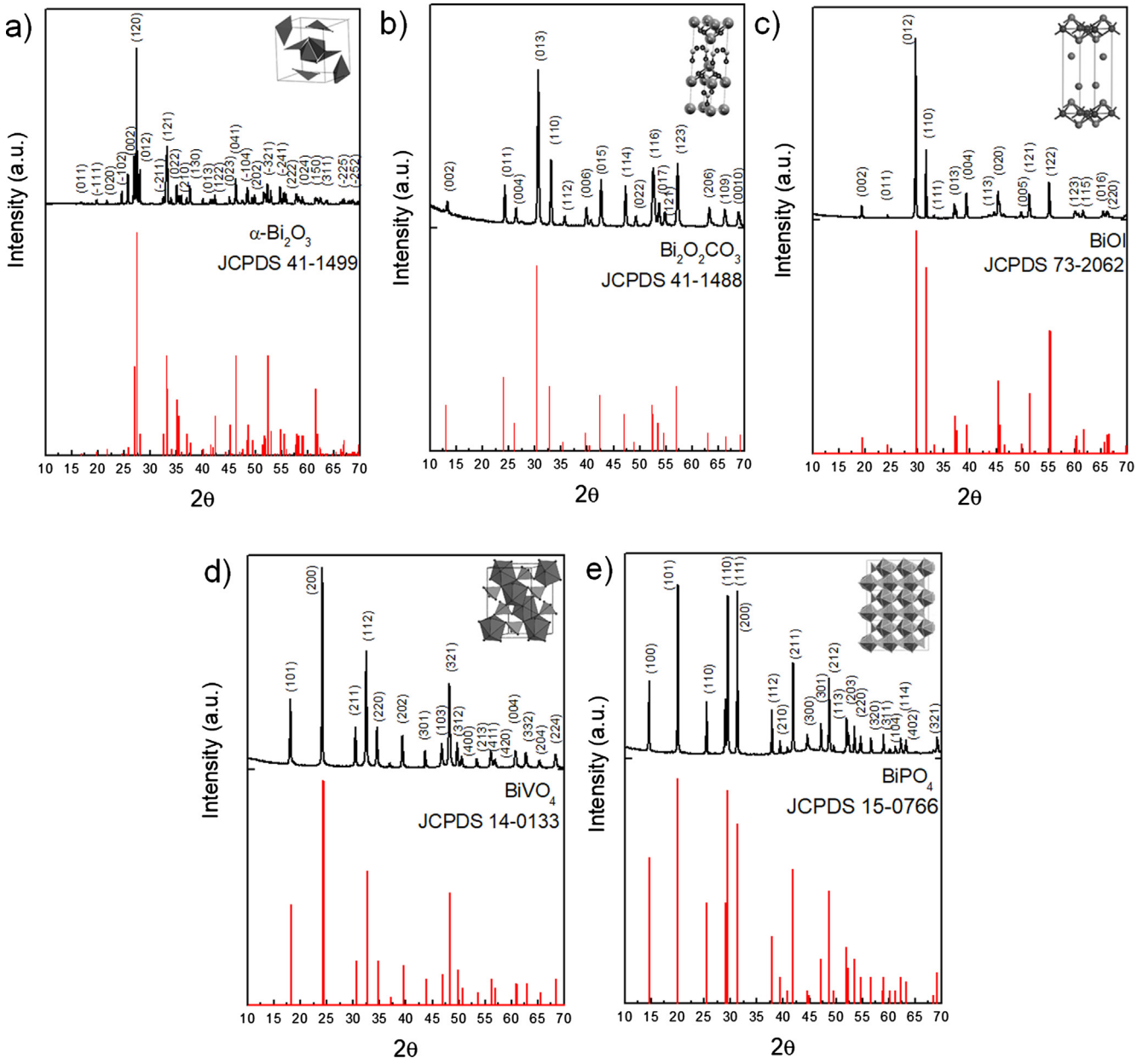

Fig. 1. X-ray powder diffraction of the bismuth-based photocatalysts.

Table 1
Physicochemical properties of bismuth-based photocatalysts.

Photocatalyst	Crystal structure	Crystallite size (nm)	Band gap (eV)	S_{BET} ($m^2\ g^{-1}$)	pH_{PZC}
Bi_2O_3	Monoclinic	65	2.8	1	4.5
$Bi_2O_2CO_3$	Tetragonal	27	3.3	19	11.5
BiOI	Tetragonal	47	2.0	4	5.6
$BiVO_4$	Tetragonal	46	2.7	2	3.5
$BiPO_4$	Hexagonal	68	4.1	5	4.6

obtained was III-type and it is characteristic of non-porous materials with low energy of adsorption [41]. Conversely, the $Bi_2O_2CO_3$ sample showed a different behavior, which exhibited a hysteresis in the interval 0.73–0.97 of relative pressure (see Fig. 5a), typical of mesoporous materials (IV-type). In order to corroborate the pore size in the $Bi_2O_2CO_3$ sample, a BJH plot was constructed, whose distribution is shown in Fig. 5b. According to this data, the mean pore diameter of $Bi_2O_2CO_3$ was 4.8 nm.

The specific surface area of samples was measured from the adsorbed N_2 volume determined with N_2 isotherms. In general, the non-porous bismuth-samples developed lower surface areas (<5 $m^2\ g^{-1}$), while the $Bi_2O_2CO_3$ sample presented the highest surface area (19 $m^2\ g^{-1}$) (Table 1).

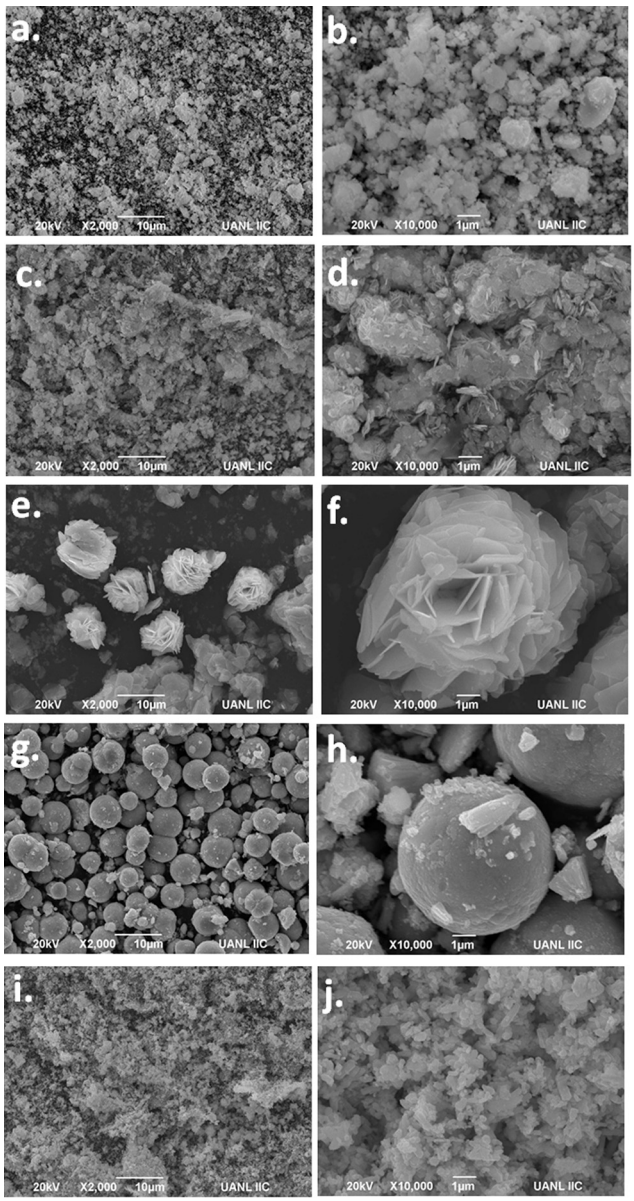

Fig. 2. SEM images of a-b. Bi_2O_3, c-d. $Bi_2O_2CO_3$, e-f. BiOI, g-h. $BiVO_4$, and i-j. $BiPO_4$.

3.5. Zeta potential

The determination of the point of zero charge (pH_{PZC}) is substantial to predict the charge on the material surface during the photooxidation reactions. This data is very important since the photocatalysis occurs on the surface and its performance can be greatly influenced by its ability to adsorb the pollutant, in this case methylene blue. In Fig. 6 can be seen the variation of zeta potential vs pH of the bismuth-photocatalysts. In particular, the pH_{PZC} increased as follows: $Bi_2O_2CO_3$ (11.5) > BiOI (5.6) > $BiPO_4$ (4.6) > Bi_2O_3 (4.5) > $BiVO_4$ (3.5). At pH values lower than pH_{PZC}, the materials have a positive charge, whereas, higher pH promotes the formation of a negative charge on the materials. It is worth mentioning that the methylene blue molecule, suggested by the ISO 10678:2010 norm for the evaluation of self-cleaning surfaces, is a cationic dye, which adsorption is favored when the photocatalyst surface is negatively charged [42].

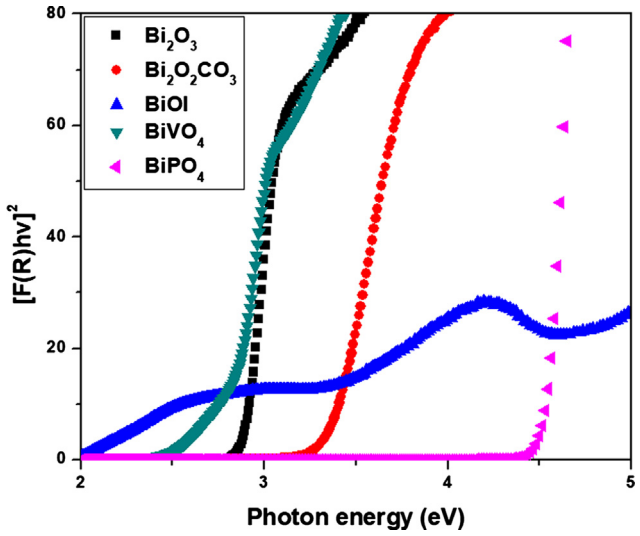

Fig. 3. Kubelka-Munk diffuse reflectance spectrum of Bi_2O_3, $Bi_2O_2CO_3$, BiOI, $BiVO_4$, and $BiPO_4$.

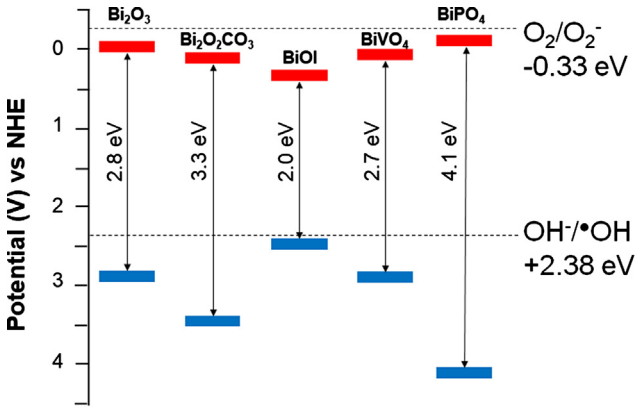

Fig. 4. Theoretical conduction and valence band positions of Bi_2O_3, $Bi_2O_2CO_3$, BiOI, $BiVO_4$, and $BiPO_4$.

3.6. Photocatalytic self-cleaning experiments

3.6.1. Powders

In a first step, it was investigating the self-cleaning efficiency of the bismuth-photocatalysts in powder form. The efficiency after 3 h of irradiation was calculated and it is shown in Fig. 7. The error bars represent the standard deviation for the photocatalytic activity based on the data repeatability of three measurements. For reference, a photolysis experiment without any photocatalyst was performed, which demonstrated the stability of the methylene blue molecule under the irradiation of the halogen lamp used. All the studied bismuth-photocatalysts showed activity for the removal of MB in aqueous solution, whose efficiency followed the tendency: $Bi_2O_2CO_3$ (70%) > BiOI (45%) > $BiVO_4$ (27%) > $BiPO_4$ (17%) > Bi_2O_3 (11%).

The highest photocatalytic efficiency obtained with the $Bi_2O_2CO_3$ photocatalyst can be associated with its physical and chemical properties, such as low particle size and high specific surface area. A nanometric particle size of photocatalyst is associated to several advantages that increase the photocatalytic efficiency of the materials, i.e., a low particle size favors a growth in the surface area, which increase the number of pollutant species (MB) that react on the photocatalyst surface. In addition, the lowest particle size

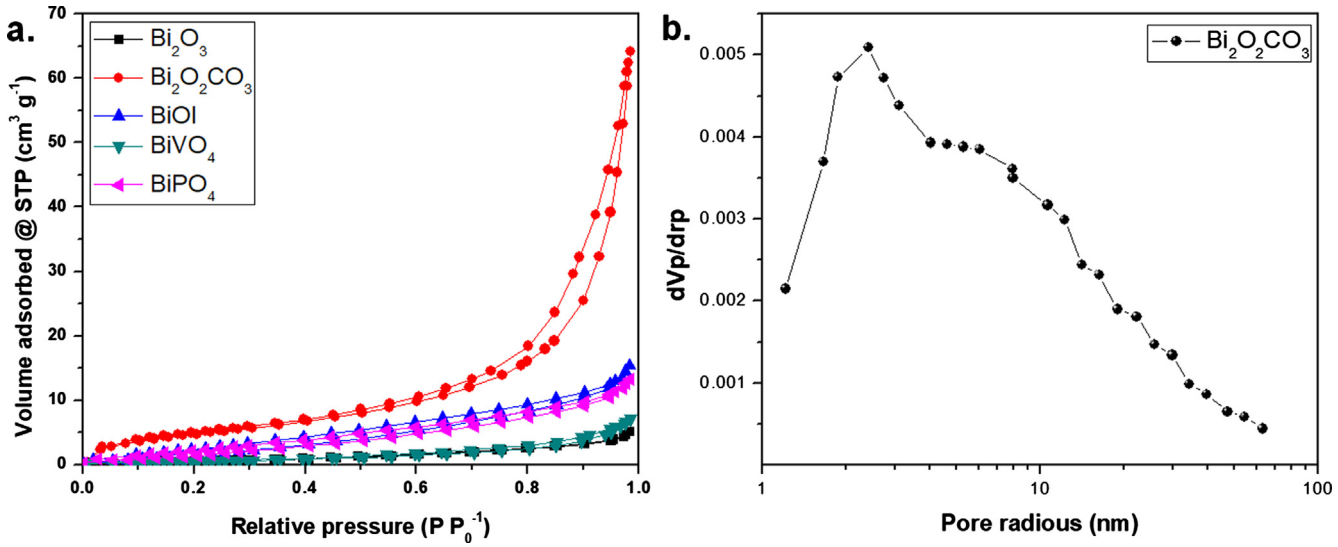

Fig. 5. a. N_2 isotherms of Bi_2O_3, $Bi_2O_2CO_3$, BiOI, $BiVO_4$, $BiPO_4$, and b. BJH plot of $Bi_2O_2CO_3$.

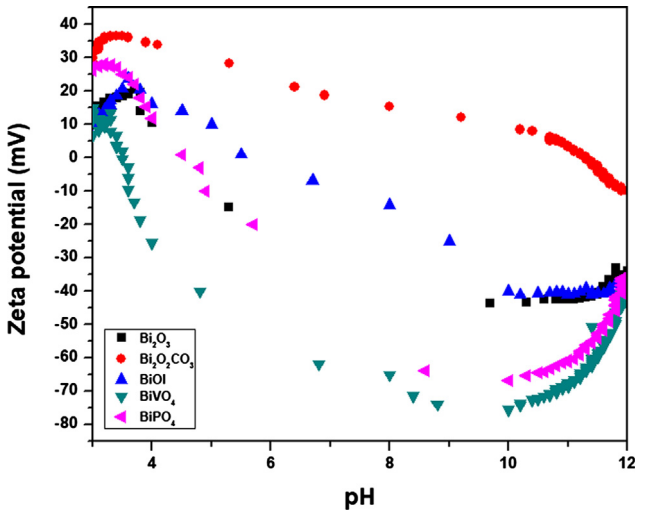

Fig. 6. Zeta potential vs pH curves of Bi_2O_3, $Bi_2O_2CO_3$, BiOI, $BiVO_4$, $BiPO_4$.

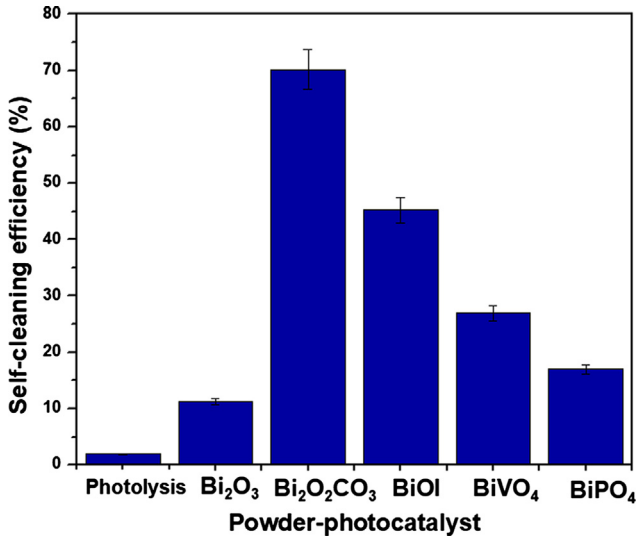

Fig. 7. Self-cleaning efficiency of bismuth-photocatalysts in *powder* form after 3 h of irradiation.

of $Bi_2O_2CO_3$ enhances the charge transfer in the semiconductor promoting more available holes to oxidize the pollutant and thus, maintaining clean the surface. Also, the best photocatalytic activity of $Bi_2O_2CO_3$ can be attributed to its negatively charged surface (pH_{PZC} = 11.5) at the pH of the experiments. In this sense, the cationic dye (MB) can be adsorbed on the $Bi_2O_2CO_3$ surface (negatively charged) through a strong electrostatic attraction. This interaction can be beneficial for enhancing the MB adsorption and thereby, increasing the self-cleaning efficiency. On the other hand, Bi_2O_3 showed the lowest efficiency, which can be attributed to its low surface area, high particle size, and acidic surface. These factors can promote an electrostatic repulsion between the positively charged Bi_2O_3 and the cationic dye. $BiPO_4$ also showed a low photocatalytic activity that could be related to its relatively wide band gap (4.1 eV). In this context, in spite of the irradiation source used emits from 300 to 900 nm, its contribution at lower wavelengths ($\lambda < 400$ nm) is not significant, which does not favor its activation under these experimental conditions.

Another important factor that affects the photocatalytic efficiency is the crystal structure of materials. In the scientific literature, there are some reports that have correlated the photocatalytic activity with the distortion of the crystal structures of photocatalysts. In particular, this effect has been reported for $BiVO_4$ and $BiPO_4$, which exhibited an arrangement composed of BiO_8 dodecahedral with VO_4 and PO_4 tetrahedral units, respectively [43,44]. Both photocatalysts exhibited a high distortion in their VO_4 and PO_4 units that can affect the dipole moment in the structure, which eventually decreases the efficiency in the charge transfer. Instead, α-Bi_2O_3 can also present a certain degree of distortion. Its structure is composed of [BiO_5E] half-octahedron distorsioned units, where E denotes an unshared electron pair [45]. Therefore, according to the photocatalytic efficiency shown in Fig. 7, it seems that the distortion had a negative impact on this reaction. On the other hand, the rest of photocatalysts: $Bi_2O_2CO_3$ and BiOI show a laminar structure composed of $(Bi_2O_2)^{2+}$ layers between slabs of CO_3^{2-} and I^-, respectively, stacked one above the other by nonbonding van der Waals interaction through along [0 0 1] direction [46,47]. This laminar morphology can favor the adsorption of different types of pollutants over the photocatalyst, which greatly improves the efficiency of the self-cleaning application. In addition,

the distortion in these structures is not significant compared to α-Bi_2O_3, $BiVO_4$, and $BiPO_4$.

3.6.2. Photocatalytic self-cleaning coatings

The self-cleaning efficiency of the photocatalytic coatings fabricated with fly ash and powders of the five bismuth-based photocatalysts was investigated following the standard ISO 10678:2010. Fig. 8 shows the self-cleaning performance of the photocatalytic coatings after 7 days of curing. In general, the photocatalytic activity followed the same tendency as the observed for the powders, whose results demonstrated the efficacy of $Bi_2O_2CO_3$ in this application. The best result was 49% after 3 h of continuous irradiation. For reference, the coating without was studied without any photocatalysts, whose results confirmed the null photocatalytic activity of the fly ash components (SiO_2, CaO, MgO, etc.) submitted to an alkaline activation [36]. For reference purpose, it was performed an additional experiment using TiO_2 P-25 as coating, which self-cleaning efficiency was only 28% under the same conditions. The lower efficiency obtained with the TiO_2 P-25 could be associated to its low activation under the light source employed.

Additionally, the effect of curing time and stability of the self-cleaning efficiency of the coatings were investigated. For this purpose, two additional experiments were performed after 14 and 28 days. As it is shown in Fig. 9, a decrease up to 38% of the initial self-cleaning efficiency, it was observed during the period of paste-hydration. This decrease could be attributed to several factors. For example, it has been reported that the kinetics of the reaction can be limited by mass transfer of reactants or photons due to the transition metal elements in the fly ash that can absorb or block the irradiation [48]. Another cause can be the pore structure change (shrinkage) during the paste hydration process [49], promoting a decrease in the surface area and thus, lower adsorption of target pollutants. In order to corroborate this, the surface area of the photocatalytic coating was measured after 0, 7, and 14 days, which results were 4.5, 3.5, and 2.1 $m^2\ g^{-1}$, respectively. The results indicated a decrease in surface area up to 53%, which could limit the self-cleaning efficiency, shown in Fig. 9.

Once the coating was evaluated after 28 days, it was washed with distilled water in order to restore the photocatalytic activity. After this experiment, the photocatalytic activity of the coating increased to 41%, which was 36% higher than the corresponding value after its evaluation at 28 days. Without washing, the generation of relatively stable reaction intermediates can lower the efficiency of the self-cleaning coating and eventually, stop the reaction through blocking active sites.

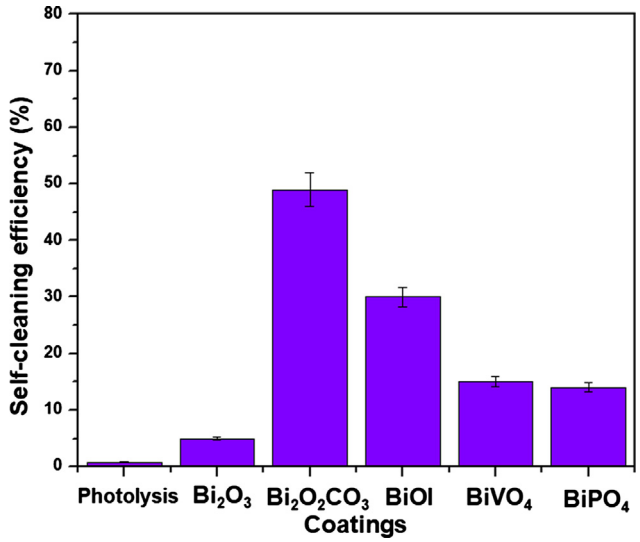

Fig. 8. Self-cleaning efficiency of the photocatalytic *coatings* after 3 h of irradiation.

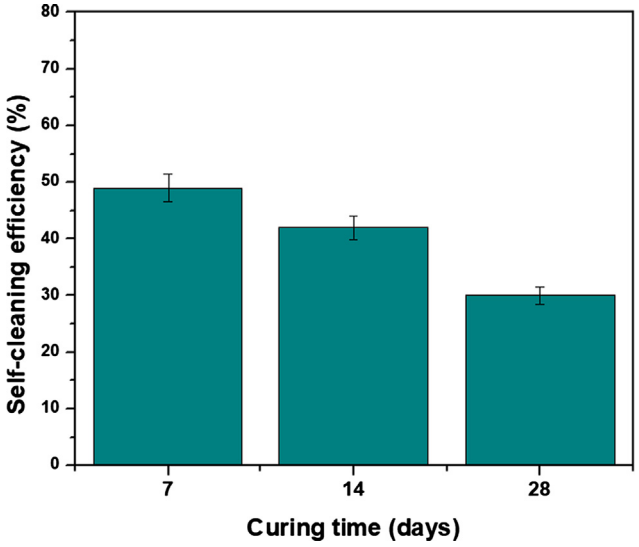

Fig. 9. Self-cleaning efficiency of the photocatalytic *coating with 3% wt. of* $Bi_2O_2CO_3$ at different curing ages.

It is important to note that the mechanical properties of the substrate were not modified after the incorporation of the coating, which resistance was 250 kg_f/cm^2.

4. Conclusions

Alternative cementitious photocatalytic materials were fabricated with fly ashes, alkaline activators and Bi_2O_3, $Bi_2O_2CO_3$, BiOI, $BiVO_4$, $BiPO_4$ photocatalysts for the first time. The photocatalytic low-cost coatings obtained can maintain a clean surface preventing the soil phenomena without affecting the mechanical properties on the concrete.

All the bismuth-photocatalysts exhibited self-cleaning activity to degrade organic molecules under light irradiation. In particular, $Bi_2O_2CO_3$ showed the highest efficiency as a powder (70%). This material also showed the best activity (49%) when it was mixed with fly ashes and alkaline activators as coating on concrete. A high surface area, low particle size, and a negative charge surface were the key factors in determining the photocatalytic activity. The self-cleaning ability of the coating restored with water after 28 days of curing.

Declaration of Competing Interest

None declared.

Acknowledgments

The authors wish to thank CONACYT and UANL for financial support for this research through the following projects: Cátedras CONACYT 1060, CONACYT-CB-2014-237049, CONACYT-PDCPN-2015-487, CONACYT-NRF-2016-278729, CONACYT-FC-1725, PAIFIC/2018-9, PAIFIC/2018-5, UANL-CA-244 PROFIDES Desarrollo de materiales ambientales ID 63185, and Verano Científico y Tecnológico 2018 (PROVERICYT).

References

[1] R. Paolini, D. Borroni, M.P. Pedeferri, M.V. Diamanti, Self-cleaning building materials: the multifaceted effects of titanium dioxide, Constr. Build. Mater. 182 (2018) 126–133, https://doi.org/10.1016/j.conbuildmat.2018.06.047.

[2] P. Munafò, E. Quagliarini, G.B. Goffredo, F. Bondioli, A. Licciulli, Durability of nano-engineered TiO2 self-cleaning treatments on limestone, Constr. Build. Mater. 65 (2014) 218–231, https://doi.org/10.1016/j.conbuildmat.2014.04.112.

[3] A. Andaloro, E.S. Mazzucchelli, A. Lucchini, M.P. Pedeferri, Photocatalytic self-cleaning coatings for building facade maintenance. Performance analysis through a case-study application, J. Facade Des. Eng. 4 (2016) 115–129, https://doi.org/10.7480/jfde.2016.4-3.1148.

[4] E. Luévano-Hipólito, A. Martínez-de la Cruz, Photocatalytic stucco for NOx removal under artificial and by real weatherism, Constr. Build. Mater. 174 (2018) 302–309, https://doi.org/10.1016/j.conbuildmat.2018.04.095.

[5] J. Chen, S.-C. Kou, C.-S. Poon, Photocatalytic cement-based materials: comparison of nitrogen oxides and toluene removal potentials and evaluation of self-cleaning performance, Build. Environ. 46 (2011) 1827–1833, https://doi.org/10.1016/j.buildenv.2011.03.004.

[6] Maria Vittoria Diamanti, Marco Ormellese, MariaPia Pedeferri, Characterization of photocatalytic and superhydrophilic properties of mortars containing titanium dioxide, Cem. Concr. Res. 38 (2008) 1349–1353, https://doi.org/10.1016/j.cemconres.2008.07.003.

[7] F. Bondioli, R. Taurino, A.M. Ferrari, Functionalization of ceramic tile surface by sol–gel technique, J. Colloid. Interface Sci. 334 (2009) 195–201, https://doi.org/10.1016/j.jcis.2009.02.054.

[8] L. Pinho, M. Rojas, M.J. Mosquera, Ag-SiO2-TiO2 nanocomposite coatings with enhanced photoactivity for self-cleaning application on building materials, Appl. Catal. B. 178 (2015) 144–154, https://doi.org/10.1016/j.apcatb.2014.10.002.

[9] M. Luna, Juan J. Delgado, M.L. Almoraima Gil, M.J. Mosquera, TiO2-SiO2 coatings with a low content of AuNPs for producing self-cleaning building materials, Nanomaterials 8 (2018) 177–203, https://doi.org/10.3390/nano8030177.

[10] J.D. Cohen, G.A.S. Gallego, J.I. Tobón, Evaluation of photocatalytic properties of Portland cement blended with titanium oxynitride (TiO2−xNy) nanoparticles, Coatings 5 (2015) 465–476, https://doi.org/10.3390/coatings5030465.

[11] R.K. Nath, M.F.M. Zain, A.A.H. Kadhum, A.B.M.A. Kaish, An investigation of LiNbO3 photocatalyst coating on concrete surface for improving indoor air quality, Constr. Build. Mater. 54 (2014) 348–353, https://doi.org/10.1016/j.conbuildmat.2013.12.072.

[12] E. Luévano-Hipólito, A. Martínez-de la Cruz, Q.L. Yu, H.J.H. Brouwers, Synthesis, characterization, and photocatalytic activity of WO3/TiO2 for NO removal under UV and visible light irradiation, Mater. Chem. Phys. 148 (2014) 208–213, https://doi.org/10.1016/j.matchemphys.2014.07.034.

[13] J. Hou, C. Yang, Z. Wang, W. Zhou, S. Jiao, H. Zhu, In situ synthesis of α–β phase heterojunction on Bi2O3 nanowires with exceptional visible-light photocatalytic performance, Appl. Catal. B. 142–143 (2013) 504–511, https://doi.org/10.1016/j.apcatb.2013.05.050.

[14] H. Cheng, B. Huang, K. Yang, Z. Wang, X. Qin, X. Zhang, Y. Dai, Facile template-free synthesis of Bi2O2CO3 hierarchical microflowers and their associated photocatalytic activity, ChemPhysChem 11 (2010) 2167–2173, https://doi.org/10.1002/cphc.200901017.

[15] S. Song, H. Yang, C. Zhou, J. Cheng, Z. Jiang, Z. Lu, J. Miao, Underwater superoleophobic mesh based on BiVO4 nanoparticles with sunlight-driven self-cleaning property for oil/water separation, Chem. Eng. J. 320 (2017) 342–351, https://doi.org/10.1016/j.cej.2017.03.071.

[16] L. Zhou, W. Wang, L. Zhang, Ultrasonic-assisted synthesis of visible-light-induced Bi2MO6 (M = W, Mo) photocatalysts, J. Mol. Catal. A 268 (2007) 195–200, https://doi.org/10.1016/j.molcata.2006.12.026.

[17] H. Gnayem, Y. Sasson, Hierarchical nanostructured 3D flowerlike $BiOCl_xBr_{1-x}$ semiconductors with exceptional visible light photocatalytic activity, ACS Catal. 3 (2013) 186–191, https://doi.org/10.1021/cs3005133.

[18] B. Shi, H. Yin, T. Li, J. Gong, S. Lv, Q. Nie, Synthesis of surface oxygen-deficient BiPO4 nanocubes with enhanced visible light induced photocatalytic activity, Mat. Res. 20 (2017) 619–627, https://doi.org/10.1590/1980-5373-mr-2016-0569.

[19] K. Liang, C. Wang, X. Xu, J. Leng, H. Ma, Capacitive and photocatalytic performance of Bi2S3 nanostructures synthesized by solvothermal method, Phys. Lett. A 381 (2017) 652–657, https://doi.org/10.1016/j.physleta.2016.12.005.

[20] X. Meng, Z. Zhang, Facile synthesis of BiOBr/Bi2WO6 heterojunction semiconductors with high visible-light-driven photocatalytic activity, J. Photochem. Photobiol. A 310 (2015) 33–44, https://doi.org/10.1016/j.jphotochem.2015.04.024.

[21] E. Luévano-Hipólito, A. Martínez-de la Cruz, Q.L. Yu, H.J.H. Brouwers, Photocatalytic removal of nitric oxide by Bi2Mo3O12 prepared by co-precipitation method, Appl. Catal. A 468 (2013) 322–326, https://doi.org/10.1016/j.apcata.2013.09.013.

[22] R. Chen, C. Zhua, J. Lu, J. Xiao, Y. Lei, Z. Yu, BiVO4/α-Fe2O3 catalytic degradation of gaseous benzene: preparation, characterization and photocatalytic properties, Appl. Surf. Sci. 427 (2018) 141–147, https://doi.org/10.1016/j.apsusc.2017.08.153.

[23] Q. Zhang, S. Yuan, B. Xu, Y. Xu, K. Cao, Z. Jin, C. Qiu, M. Zhang, C. Su, T. Ohno, A facile approach to build Bi2O2CO3/PCN nanohybrid photocatalysts for gaseous acetaldehyde efficient removal, Catal. Today 315 (2018) 184–193, https://doi.org/10.1016/j.cattod.2018.03.071.

[24] W.C. Huo, X. Dong, J.Y. Li, M. Li, X.Y. Liu, Y.X. Zhang, F. Dong, Synthesis of Bi2WO6 with gradient oxygen vacancies for highly photocatalytic NO oxidation and mechanism study, Chem. Eng. J. 361 (2019) 129–138, https://doi.org/10.1016/j.cej.2018.12.071.

[25] W. He, Y. Sun, G. Jiang, Y. Li, X. Zhang, Y. Zhang, Y. Zhou, F. Dong, Defective Bi4MoO9/Bi metal core/shell heterostructure: Enhanced visible light photocatalysis and reaction mechanism, Appl. Catal. B: Environ. 239 (2018) 619–627, https://doi.org/10.1016/j.apcatb.2018.08.064.

[26] J. Li, W. Zhang, M. Ran, Y. Sun, H. Huang, F. Dong, Synergistic integration of Bi metal and phosphate defects on hexagonal and monoclinic BiPO4: enhanced photocatalysis and reaction mechanism, Appl. Catal. B: Environ. 243 (2019) 313–321, https://doi.org/10.1016/j.apcatb.2018.10.055.

[27] W.W. Anku, S.O.B. Oppong, P.P. Govender, Bismuth-based nanoparticles as photocatalytic materials, IntechOpen (2017), https://doi.org/10.5772/intechopen.75104.

[28] S.M.A. El-Gamal, F.I. El-Hosiny, M.S. Amin, D.G. Sayed, Ceramic waste as an efficient material for enhancing the fire resistance and mechanical properties of hardened Portland cement pastes, Constr. Build. Mater. 154 (2017) 1062–1078, https://doi.org/10.1016/j.conbuildmat.2017.08.040.

[29] A. Hanif, Z. Lu, Z. Li, Utilization of fly ash cenosphere as lightweight filler in cement-based composites – a review, Constr. Build. Mater. 144 (2017) 373–384, https://doi.org/10.1016/j.conbuildmat.2017.03.188.

[30] S. Moutinho, C. Costa, Â. Cerqueira, F. Rocha, A. Velosa, Geopolymers and polymers in the conservation of tile facades, Constr. Build. Mater. 197 (2019) 175–184, https://doi.org/10.1016/j.conbuildmat.2018.11.058.

[31] J. Torkaman, A. Ashori, A.S. Momtazi, Using wood fiber waste, rice husk ash, and limestone powder waste as cement replacement materials for lightweight concrete blocks, Constr. Build. Mater. 50 (2014) 432–436, https://doi.org/10.1016/j.conbuildmat.2013.09.044.

[32] M.S. Morsy, S.H. Alsayed, Y.A. Salloum, Development of eco-friendly binder using metakaolin-fly ash–lime-anhydrous gypsum, Constr. Build. Mater. 35 (2012) 772–777, https://doi.org/10.1016/j.conbuildmat.2012.04.142.

[33] A.K. Saha, Effect of class F fly ash on the durability properties of concrete, Sustain. Environ. Res. 28 (2018) 25–31, https://doi.org/10.1016/j.serj.2017.09.001.

[34] R. Siddique, P. Aggarwal, Y. Aggarwal, Influence of water/powder ratio on strength properties of self-compacting concrete containing coal fly ash and bottom ash, Constr. Build. Mater. 29 (2012) 73–81, https://doi.org/10.1016/j.conbuildmat.2011.10.035.

[35] S. Aydın, Ç. Karatay, B. Baradan, The effect of grinding process on mechanical properties and alkali–silica reaction resistance of fly ash incorporated cement mortars, Powder Technol. 197 (2010) 68–72, https://doi.org/10.1016/j.powtec.2009.08.020.

[36] E. Luévano-Hipólito, A. Martínez-de la Cruz, Enhanced photocatalytic activity of TiO2 rutile by coupling with fly ashes for the removal of NO gases, Ind. Eng. Chem. Res. 55 (2016) 11512–11519, https://doi.org/10.1021/acs.iecr.6b03302.

[37] M.A. Butler, D.S. Ginley, Prediction of flatband potentials at semiconductor-electrolyte interfaces from atomic electronegativities, J. Electrochem. Soc. 125 (1978) 228–232, https://doi.org/10.1149/1.2131419.

[38] J. Zhang, Y. Nosaka, Mechanism of the OH radical generation in photocatalysis with TiO2 of different crystalline types, J. Phys. Chem. C 118 (2014) 10824–10832, https://doi.org/10.1021/jp501214m.

[39] D.S. Bhatkhande, V.G. Pangarkar, A.A.C.M. Beenackers, Photocatalytic degradation for environmental applications – a review, J. Chem. Technol. Biot. 77 (2001) 102–116, https://doi.org/10.1002/jctb.532.

[40] S.L. Suib, New and Future Developments in Catalysis, Catalysis for Remediation and Environmental Concerns, Elsevier, 2003.

[41] F. Rouquerol, J. Rouquerol, K. Sing, Adsorption by Powders and Porous Solids: Principles, Methodology and Applications, Academic Press, Waltham, 1999.

[42] A.H. Jawad, A.F.M. Alkarkhi, N.S.A. Mubarak, Photocatalytic decolorization of methylene blue by an immobilized TiO2 film under visible light irradiation: optimization using response surface methodology (RSM), Desalin. Water Treat. 56 (2015) 161–172, https://doi.org/10.1080/19443994.2014.934736.

[43] C. Pan, D. Li, X. Ma, Y. Chen, Y. Zhu, Effects of distortion of PO4 tetrahedron on the photocatalytic performances of BiPO4, Catal. Sci. Technol. 1 (2011) 1399–1405, https://doi.org/10.1039/C1CY00261A.

[44] S. Tokunaga, H. Kato, A. Kudo, Selective preparation of monoclinic and tetragonal BiVO4 with scheelite structure and their photocatalytic properties, Chem. Mater. 13 (2001) 4624–4628, https://doi.org/10.1021/cm0103390.

[45] J. Shin, J.-M. You, J.Z. Lee, R. Kumar, L. Yin, J. Wang, Y.S. Meng, Deposition of ZnO on bismuth species towards a rechargeable Zn-based aqueous battery, Phys. Chem. Chem. Phys. 18 (2016) 26376–26382, https://doi.org/10.1039/C6CP04566A.

[46] H. Huang, N. Tian, S. Jin, Y. Zhang, S. Wang, Syntheses, characterization and nonlinear optical properties of a bismuth subcarbonate Bi2O2CO3, Solid State Sci. 30 (2014) 1–5, https://doi.org/10.1016/j.solidstatesciences.2014.01.010G.

[47] W.-W. Dai, Z.-Y. Zhao, Electronic structure and optical properties of BiOI as a photocatalyst driven by visible light, Catalysts 6 (2016) 133–148, https://doi.org/10.1021/acs.inorgchem.5b01714.

[48] J. Chen, C.-S. Poon, Photocatalytic cementitious materials: influence of the microstructure of cement paste on photocatalytic pollution degradation, Environ. Sci. Technol. 43 (2009) 8948–8952, https://doi.org/10.1021/es902359s.

[49] J. Chen, C.-S. Poo, Photocatalytic activity of titanium dioxide modified concrete materials – influence of utilizing recycled glass cullets as aggregates, J. Environ. Manage. 90 (2009) 3436–3442, https://doi.org/10.1016/j.jenvman.2009.05.029.